Author Manuscript

Author Manuscript

Author Manuscript

Author Manuscript

HHS Public Access

Author manuscript

J Immunol. Author manuscript; available in PMC 2021 October 15.

Published in final edited form as:

J Immunol. 2020 October 15; 205(8): 2231–2242. doi:10.4049/jimmunol.1901533.

Small Molecule Inhibitor of 8-oxoguanine DNA Glycosylase 1 Regulates Inflammatory Responses during *P. aeruginosa* Infection

Shugang Qin[1,2], **Ping Lin**[2,3], **Qun Wu**[2,6], **Qinqin Pu**[1,2], **Chuanmin Zhou**[7], **Biao Wang**[2], **Pan Gao**[1,2], **Zhihan Wang**[2,4], **Ashley Gao**[2], **Madison Overby**[2], **Jinliang Yang**[1], **Jianxin Jiang**[3], **David L. Wilson**[5], **Yu-ki Tahara**[5], **Eric T. Kool**[5,*], **Zhenwei Xia**[6,*], **Min Wu**[2,*]

[1]State Key Laboratory of Biotherapy and Cancer Center, West China Hospital, Sichuan University, and Collaborative Innovation Center for Biotherapy, Chengdu, Sichuan 610041, China

[2]Department of Biomedical Sciences, School of Medicine and Health Sciences, University of North Dakota, Grand Forks, North Dakota 58203, USA.

[3]State Key Laboratory of Trauma, Burns and Combined Injury, Institute of Surgery Research, Daping Hospital, The Third Military Medical University, Chongqing 400042, China.

[4]West China School of Basic Medical Sciences & Forensic Medicine, Sichuan University, Chengdu, Sichuan 610041, China.

[5]Department of Chemistry, Stanford Cancer Institute, and ChEM-H Institute, Stanford University, Stanford, CA 94305, USA.

[6]Department of Pediatrics, Ruijin Hospital affiliated to Shanghai Jiao Tong University School of Medicine, Shanghai, China.

[7]Wuhan University School of Health Sciences, Wuhan, Hubei Province, 430071, P. R. China.

Abstract

The DNA repair enzyme 8-oxoguanine DNA glycosylase 1 (OGG1), which excises 8-oxo-7,8-dihydroguanine (8-oxoG) lesions induced in DNA by reactive oxygen species, has been linked to the pathogenesis of lung diseases associated with bacterial infections. A recently developed small molecule, SU0268, has demonstrated selective inhibition of OGG1 activity; however, its role in attenuating inflammatory responses has not been tested. Here, we report that SU0268 has a favorable effect on bacterial infection both in mouse alveolar macrophages (MH-S cells) and in C57BL/6 wild-type mice by suppressing inflammatory responses, particularly promoting type I interferon responses. SU0268 inhibited pro-inflammatory responses during *P. aeruginosa* (PA14) infection, which is mediated by the KRAS-ERK1-NF-κB signaling pathway. Furthermore,

*Corresponding authors: Min Wu, min.wu@med.und.edu; Zhenwei Xia, xzw10484@rjh.com.cn; Eric T. Kool, kool@stanford.edu.

Author contributions

S.Q., P.L., E.T.K. Z.X., J.J., C.Z., B.W., D.W., P.Q., Y.T and M.W. designed the project and wrote the manuscript. P.L., Q.W., Z.W., A.G., M.O., J.Y., P.G and S.Q. designed and performed most of the experiments. E.T.K. Y.T., D.W., M.W., Z.X., and S.Q. analyzed data.

Footnotes

Disclosures

The authors have no financial conflicts of interest.

Author Manuscript Author Manuscript Author Manuscript Author Manuscript

SU0268 induces the release of type I interferon by the mtDNA-cGAS-STING-IRF3-IFNβ axis, which decreases bacterial loads and halts disease progression. Collectively, our results demonstrate that the small-molecule inhibitor of OGG1 (SU0268) can attenuate excessive inflammation and improve mouse survival rates during PA14 infection. This strong anti-inflammatory feature may render the inhibitor as an alternative treatment for controlling severe inflammatory responses to bacterial infection.

Keywords

P. aeruginosa aeruginosa; 8-oxoguanine DNA glycosylase 1; cGAS; IRF3; mtDNA

Introduction

P. aeruginosa aeruginosa (*P. aeruginosa*) is an opportunistic pathogen that causes many serious infectious diseases (1). Lung fibrosis and chronic lung injury, which can extensively induce other lung diseases and accelerate disease progression, are two abundant outcomes secondary to *P. aeruginosa* infection, which is difficult to treat and eradicate invading pathogens (2). Numerous studies have shown that *P. aeruginosa* infection is positively associated with excessive activation of inflammation (3). Therefore, regulation of the inflammatory response is crucial for the treatment of *P. aeruginosa* infections and associated lung diseases (4).

Reactive oxygen species (ROS) that are generated during bacterial infection induces genome damage by the formation of oxidatively damaged DNA bases, the most frequent of which is 8-oxo-7,8-dihydroguanine (8-oxoG) (5, 6). To ameliorate harmful mutagenic effects of this damage, the base 8-oxoG is excised from genomic and mitochondrial DNA by 8-oxoguanine DNA glycosylase-1 (OGG1) through the DNA base excision repair (BER) pathway (7). OGG1 is a DNA repair enzyme that is closely linked to oxidative stress and inflammation (8). Mice engineered to lack the OGG1 enzyme develop normally (9). Although they accumulate higher levels of 8-oxoG in their DNA, they are otherwise relatively healthy and exhibit normal lifespans (10). Importantly, in tests of inflammation, *Ogg1*$^{-/-}$ mice were shown in an early study to blunt pro-inflammatory responses to lipopolysaccharide (LPS) and allergens (11). The mice showed a lowered extent of neutrophil infiltration, decreased levels of Th1 cytokines IL-12 and TNF-α, and elevated levels of protective Th2 cytokines IL-4 and IL-10 (12).

Multiple connections between the function of OGG1 and inflammation have been documented. DNA promoter regions binding by OGG1 increased the expression levels of chemokines/cytokines, including *Cxcl-2* and TNF-α (8, 13). Thus, the prevention of DNA binding by a small molecule OGG1 inhibitor may be expected to inhibit this pro-inflammatory signaling. Efforts to develop OGG1 inhibitors have been reported recently, including compound O8, which inhibits DNA lyase activities of OGG1 but does not inhibit DNA binding (14), and SU0268, which inhibits DNA binding and base excision by the enzyme (15). Recently, Helleday and coworkers reported the development of a third small-molecule inhibitor of OGG1, TH5487, and tested it in a mouse model of inflammation

Author Manuscript Author Manuscript Author Manuscript Author Manuscript

induced by challenges with LPS or TNF-α. The study documented that TH5487 decreased levels of pro-inflammatory cytokines and chemokines, including IL-6, *Tnf*, and Cxcl2, and did so in a dose-dependent manner. It also decreased neutrophil infiltration in blood and lung fluid, and increased mouse survival rates after LPS exposure. The study provided further validation of OGG1 as a potential target for inflammation (16). To date, no studies of the effects of OGG1 inhibitors on inflammation induced by bacterial infections have been reported.

Inflammation resulting from pathogen infections is documented to be mediated, at least in part, by the intracellular release of mitochondrial and microbial DNA (17). The cyclic guanosine monophosphate (GMP)–adenosine monophosphate (AMP) synthase (cGAS), which is dependent on the binding of mitochondrial DNA (mtDNA) arising intracellularly and extracellularly, is closely related to immune function during bacterial and viral infections (18). Activated cGAS triggers the immune response through regulation of the production of type I interferons in generating the second messenger 2′3′-cyclic-GMP–AMP (cGAMP) (19). It is well known that OGG1 is involved in the process of DNA damage repair during bacterial infection. Studies have demonstrated that microbial DNA released into the cytoplasm is the major agonist of cGAS (20). However, the interactions between OGG1-mediated pathways and cGAS are currently unclear. In addition, whether OGG1 can be a potential candidate target for anti-inflammatory treatment during bacterial infection remains untested.

The compound SU0268, the most potent existing OGG1 inhibitor, is a promising small molecule candidate to probe the significance of OGG1 inhibition in downregulating clinically harmful inflammatory responses. The cell-permeable compound exhibits an *in vitro* IC_{50} of 59 nM, is selective for OGG1 over other BER enzymes, and shows low toxicity at concentrations 10 μM and below. The compound has been documented to inhibit DNA binding by OGG1, unlike previous OGG1 inhibitors. However, the activity of SU0268 in potentially influencing inflammatory responses has not yet been explored (15).

In the present study, we investigated the potential role of the compound SU0268 in modulating inflammatory response and bacterial clearance both *in vitro* and *in vivo* after *P. aeruginosa* reference strain 14 (PA14) infection. Our study demonstrates that the compound inhibits murine OGG1 activity in a mouse cell line. We found that SU0268 can potently inhibit inflammatory responses and mitigate bacterial infection. Our data provide new evidence of the relevance of OGG1 as a target in inflammation, and the compound SU0268 as a useful tool in preclinical models of this immune response.

Material and Methods

Mice

C57BL/6N mice (6–8 weeks) were purchased from the Harlan Laboratory. The mice were maintained in the animal facility at the University of North Dakota for at least two weeks before starting the experiment. Both male and female were randomly selected (age of mice ranged from 6 to 8 weeks). All animal studies were approved by the University of North

Author Manuscript Author Manuscript Author Manuscript Author Manuscript

Dakota Institutional Animal Care and Use Committee and performed in accordance with the animal care and institutional guidelines (21).

Primary cells and cell lines

Mouse primary alveolar macrophage cells (AM), bone-marrow-derived macrophage (BMDM) cells and bronchoalveolar lavage fluid (BALF) were obtained through alveolar lavage as previously described (22), cultured in RPMI 1640 (Life Technologies) supplemented with 10% FBS (Life Technologies) and incubated on a culture plate for 4 h at 37 ºC/5% CO_2 incubator to allow attachment of the macrophages. Non-adherent cells were removed by washing with sterile PBS. BMDM cells were induced into mature macrophages by adding recombinant mouse granulocyte-macrophage colony-stimulating factor (GM-CSF) (PMC2011, Thermo Fisher, Waltham, MA, USA) in the medium. Alveolar lavage fluid Murine (MH-S) cells and J744.1A cells were obtained from American Type Culture Collection (ATCC, Manassas, VA) and cultured following the manufacturer's instructions.

Bacterial and Bacterial infection assay

The wild-type *P. aeruginosa* strain PA14 was a gift from Steve Lory (Department of Molecular Genetics, Harvard Medical School). Bacteria were grown to the mid-logarithmic phase (OD 600 = 0.5–0.6) in lysogeny broth (LB) at 37°C with 220-rpm shaking. The number of bacteria was determined by measuring the OD value (1 OD = 1×10^9 cells/ml). Mammalian cells were infected PA14 in a MOI of 20:1 bacteria/cell ratio. C57BL/6N mice were anesthetized with ketamine (45 mg/kg) and intranasally infected with 6×10^6 CFU of PA14.

SU0268 treatment

SU0268, synthesized as previously described (15), was diluted in pure ethanol, then MH-S cells were treated with SU0268 for varied times before PA14 infection for 2h (pure ethanol as a control). Anesthetized C57BL/6N mice were intranasally treated with 10 mg/kg (MW= 464 g/mol) SU0268 for 12 h before infection with 6×10^6 CFU of PA14.

Cell transfection

Lipofectamine™ RNAiMAX transfection reagent (13–778-075, Invitrogen, Carlsbad, CA, USA) was dilute in 150 μl with Opti-MEM medium. Then 150 μl mixture containing 150 μl Opti-MEM medium and 9 μl siRNA or 5 ng DNA was added to the diluted transfection reagent, incubated for 5 min at room temperature. 250 μl of the mixture was added to each well. The knockdown efficiency was detected by western blotting after 48 h transfection (Fig. S4B).

3-(4,5-Dimethylthiazol-2-yl)-2,5-Diphenyltetrazolium bromide assay (MTT)

Cells were stained with trypan blue, and the number of viable cells was quantified through a cell counting plate. The concentration gradient of the SU0268 was added to the cells in a 96-well plate and incubated at 37 °C/5% CO_2 for the listed time. 20 μl of MTT solution (M6494, Thermo Fisher Scientific) (5 mg/ml, 0.5% MTT) was added to each well, and continued to culture for 4 h. Stop solution was added to dissolve the formazan product. The

Author Manuscript Author Manuscript Author Manuscript Author Manuscript

cell viability was quantified by absorbance measurement at 560 nm using a spectrometric plate reader.

OGG1 inhibition in MH-S cells

MH-S cells (ATCC) were grown in RPMI-1640 media (Gibco) supplemented with 10% FBS (Corning), 100 U/mL pen-strep (Gibco) and 0.05 M 2-mercaptoethanol (Fisher scientific) in a humidified incubator at 37 °C with 5% CO_2. For inhibitor treatment, media was supplemented with 1 μM SU0268 and replenished every 12 hours for 36 hours. For oxidative treatment, cells were treated with serum-free media containing 5 mM H_2O_2 and 100 μM $Fe(NH_4)_2(SO_4)_2$ for 1 hour prior to harvesting. To prepare lysates, cells were collected in PBS by scraping, and the protocol for the CellLytic™ NuCLEAR Extraction Kit (Sigma Aldrich) was used with Roche complete mini EDTA-free protease inhibitor tablets. Briefly, cells were grown to ~90% confluency and harvested by scraping (~5×10^7). Cells were rinsed twice with cold PBS and swelled in hypotonic lysis buffer for 15 minutes on ice (10 mM Tris, pH 7.0, with 1.5 mM $MgCl_2$, 10 mM NaCl, 0.1 M DTT and 1x protease inhibitor). Cells were lysed by repeated passage through a 25-gauge needle and the cytosolic fraction collected. Nuclear proteins were extracted from the nuclear pellet by shaking with a high salt nuclear extraction buffer for 60 minutes (20 mM HEPES, pH 7.9, with 1.5 mM $MgCl_2$, 420 mM NaCl, 0.1 M DTT, 25% glycerol and 1x protease inhibitor). The nuclear and cytosolic fractions were then combined, and total protein was determined by Bradford assay. OGG1 activity was measured in MH-S lysates (0.1 mg/mL) using the previously reported universal base excision reporter (UBER) probe system (23). Briefly, lysates were incubated with an 8-oxoG containing substrate (5 μM) and the glycosylase probe CCVJ1 (25 μM) with either SU0268 (1 μM) or a DMSO control for 4 hours prior to measuring fluorescence. Percent activity represents the enzyme activity relative to the DMSO control with background subtracted (lysate and probe without substrate).

Measurement of 8-oxoG in DNA

MH-S cells were harvested by scraping (5×10^6) and rinsed twice with PBS. Genomic DNA was isolated using a Quick-DNA Miniprep Plus Kit (Zymo Research) according to the manufacturer's instructions and concentration assessed by UV absorbance on a NanoDrop instrument (ThermoFisher). DNA was melted at 95 °C for 5 minutes, then rapidly chilled and digested with nuclease P1 (New England Biolabs) for 2 hours at 37 °C before a second heat treatment at 75 °C for 10 minutes to inactivate the enzyme. A commercial ELISA kit for 8-oxoG determination (Abcam) was used according to the manufacturer's instructions. Absorbance measurements were taken on an Infinite M1000 microplate reader (Tecan) and compared against a calibration curve. Meanwhile, the expression level of 8-oxodG was also assessed by using HT 8-oxo-dG ELISA Kit II (4380–096-K, Gaithersburg, MD, Trevigen) according to the manufacturer's instructions. Briefly, MH-S cells were treated with 2 μM SU0268 for 8 h and collected in 1.5 ml microtubes, washed two times with PBS, centrifuged at 10,000 g/min for 10 sec at 4°C, the supernatant discarded, the DNA extracted from the above-collected cell pellets by using DNeasy Blood & Tissue Kit (69504, QIAGEN) according to the manufacturer's instructions. 25 μl of 8-OHdG standards and clarified samples were added to each well (Assay diluent buffer without 8-OHdG as background control), then 25 μl of anti 8-OHdG monoclonal solution, 50 μl of diluted Goat anti-Mouse

Author Manuscript Author Manuscript Author Manuscript Author Manuscript

IgG-HRP conjugate and 50 μl of pre-warmed TACS-Sapphire™ colorimetric substrate were added sequentially to all wells except blank wells and incubated in the dark for 15 minutes at 25°C. Reactions were stopped by adding 5% phosphoric acid. The absorbance was immediately read at 450 nm.

RNA isolation and qPCR

RNA was extracted from lung tissues with Trizol reagent (Invitrogen, Carlsbad, CA) according to the manufacturer's instruction. Complementary DNA (cDNA) was obtained through reverse transcription reaction (Invitrogen). Genes were quantified by using Real-Time Quantitative PCR (qPCR) reaction (Bio-Rad, Hercules, CA, USA). The PCR primers used in the reaction are listed in Supplementary Table S1 and S2.

Measurement of inflammatory cytokines

Cytokine concentrations were measured by an ELISA kit (eBioscience, San Diego, CA, USA) in MH-S cells following the instruction of the manufacturer in 96-well plates (Corning Costar 9018). Briefly, plates were coated with 100 μl/well of capture antibody in coating buffer and incubated overnight at 4 °C. 100 μl of detection antibody with 1x ELISA/ELISPOT buffer was added to each well. Cytokine concentrations were determined with the corresponding detection of HRP-conjugated antibodies. Optical absorbance was read at 450 nm and analyzed.

Western blotting

Mouse monoclonal Abs against β-actin (sc-47778) and Horseradish peroxidase-labeled secondary antibody (sc-49395) were obtained from Santa Cruz Biotechnology. IL-1β (12242), TNF-α (5178), IL-6 (12912), cGAS (31659), p-TBK (5483), TBK (3504), IRF-3 (4302), p-IRF-3 (79945) and GEFs (4076) were purchased from Cell Signaling Technology (Danvers, MA, USA); KRAS (sc-30), NF-κB p65 (sc-8008), ERK1 p44 (sc-271291) were purchased from Santa Cruz Biotechnology (Santa Cruz, CA, USA). Cells and homogenized lung tissue were lysed in RIPA buffer containing protease inhibitor (ThermoFisher Scientific), then were denatured in 100 °C for 10 min, separated by electrophoresis on 12% SDS-PAGE gels, and then transferred to nitrocellulose transfer membranes (GE Amersham Biosciences, Pittsburgh, PA). Membranes were incubated with primary Abs overnight, then were incubated with corresponding secondary Abs conjugated to HRP (Santa Cruz Biotechnology). Finally, the relative expression levels of protein were detected using ECL reagents (Santa Cruz Biotechnology) and were quantified by Quantity One software (Bio-Rad).

Immunostaining

Cells were cultured overnight in 24-well plates containing slides. Cells were fixed with 4% paraformaldehyde (PBS) for 15 min and washed with PBS 3 times for 3 min each time. 300 μl of 0.5% Triton X-100 (diluted in PBS) was added to each well, and permeabilized for 20 min at room temperature. Then, 5% BSA was added on the slide and blocked at room temperature for 30 min. Primary antibody that was diluted in 1% BSA was added in the amount of 200 μl/well, slides were put into the wet box, and incubated overnight at 4 °C.

Author Manuscript Author Manuscript Author Manuscript Author Manuscript

Then the slides were incubated with the appropriate fluorescein-conjugated secondary Abs in the dark. For detection of released mitochondrial DNA, MH-S cells were marked by transfected plasmid TG (Coexpression of the mtDNA-binding protein transcription factor A, which was tagged with the green fluorescent protein variant mNeonGreen) and TH (Red, TOMM20-Halo) (24) (gift from Benjamin T. Kile, Department of Medical Biology, University of Melbourne), and then DAPI (Sigma-Aldrich) was used to stain the nucleus for 10 min in the dark at room temperature. The coverslips were mounted on slides with VECTASHIELD mounting medium. The images were captured with a Zeiss Meta 510 confocal microscope (Carl Zeiss, Oberkochen, Germany). NF-κB p65 (sc-8008) antibodies were purchased from Santa Cruz Biotechnology (Santa Cruz, CA, USA), and TNF-α (11948), IL-6 (12912), cGAS (31659), IRF-3 (4302) antibodies were purchased from Cell Signaling Technology (Danvers, MA, USA).

Nitroblue tetrazolium (NBT) assay

MH-S cells were placed in 96-well plates in serum-containing complete medium and were attached at 37 °C for 4 h. 1 μg/ml NBT dye (298–83-9, Sigma-Aldrich, St. Louis, MO, USA) was added to each well and incubated at 37 °C for 1 h until the color changed from yellow to purple formazan. 100 μl of stop solution (10% DMSO, 10% SDS in 50 mM HEPES buffer) was added to each well. The plate was placed at room temperature overnight to completely dissolve the formazan and the OD value read at 560 nm. Each experiment was performed in triplicate.

Dihydrodichlorofluorescein diacetate (H_2DCF-DA) assay

MH-S cells were transfected with 5 μM H_2DCF-DA staining solution (Molecular Probes, Carlsbad, CA) in a 96-well plate, incubated at 37 °C for 30 min, and fluorescence was measured by a fluorescence plate reader (BioTek, Winooski, VT) using 485 nm excitation and 528 nm emission filter. The images were captured on a Zeiss Meta 510 confocal microscope (Carl Zeiss).

Comet assay

The Comet Assay was performed by using the CometAssay® HT kit (4252–040-K, Trevigen) according to the manufacturer's instructions. Briefly, MH-S cells were treated with SU0268, then were infected with PA14; cells were then harvested and resuspended in ice-cold PBS. Cells (1×10^5/ml) were combined with low melting agarose (kept in 37°C water bath for at least 20 min to cool) at a ratio of 1:10 (v/v). Immediately afterward, 30 μl were pipetted onto the 20 well CometSlide™. Slides were laid flat at 4˚C in the dark for 10 min, immediately immersed with Lysis Solution and incubated overnight at 4°C, then were washed with unwinding Solution (pH>13). Alkaline Electrophoresis was performed at 21 Volts for 30 min, slides were immersed in the diluted staining solution containing with 50 μl SYBR® Gold for 30 min in the dark, and the images were captured with a Zeiss Meta 510 confocal microscope (Carl Zeiss, Oberkochen, Germany).

Author Manuscript Author Manuscript Author Manuscript Author Manuscript

Assessment of mitochondrial membrane potential

MH-S cells were collected in the 96-well plate. 10 μl of the JC-1 staining solution was added and incubated in the incubator for 30 min. The plate was then centrifuged at 400 g for 5 min at room temperature and the supernatant was discarded. Then, 200 μl of Assay buffer was added to each well, fluorescence values of cells were analyzed with a fluorescence plate reader. Strong fluorescence intensity with emission at 535 nm and 595 nm is typical for healthy cells but at 485 nm and 535 nm for unhealthy cells. Triplicates were performed for each sample and control (25). The images were captured with a Zeiss Meta 510 confocal microscope (Carl Zeiss, Oberkochen, Germany).

Extraction and quantification of mtDNA release in cytoplasm

MH-S and J744A.1 Cells (1×10^6) were collected, and then were washed with 1x DPBS once. Then, 1% NP-40 (100 μl) was added to each well and the cells were scraped. Lysates were placed into prelabeled microcentrifuge tubes and incubated on ice for 15 min. Lysates were spun at 13,000 rpm for 15 min at 4 °C to pellet the insoluble fraction. Supernatant (the cytosolic fraction) was transferred to a new tube and the pellet was discarded. The supernatant was used in the next step to extract cytosolic mitochondrial DNA by using DNeasy Blood & Tissue Kit (69504, QIAGEN) according to the manufacturer's instructions. Finally, the expression levels were quantified by qPCR. The following primers were used: Cytochrome c oxidase I (mtDNA gene), housekeeping gene (18S rDNA) (26, 27). The PCR primers used in the manuscript are listed in Supplementary Table S1.

Assessment of apoptosis

The cells (cell numbers $>10^5$) were collected after treatment with SU0268 for 8 h, followed by infection with PA14 for 2 h, washed twice with PBS, resuspended, and centrifuged for 4 min at 3000 r/min. 1.5 μM propidium iodide staining (V13242, Thermo Fisher Scientific) solution was added and incubated in the dark for 30 minutes at room temperature. Apoptosis was detected by flow cytometry.

Immunoprecipitation

MH-S cells were carefully washed with pre-chilled PBS 2 times. Pre-chilled RIPA lysis buffer (50 mM PH7.4 Tri-HCl, 15mM NaCl, 1mM EDTA, 0.1% NP-40, 1.25% Triton X-100, protease inhibitor) was added, and then MH-S cells were collected to sterilized 1.5 ml Eppendorf tubes using a pre-chilled scraper, then cells were centrifuged at 14,000 g/min for 15 min at 4 °C, the supernatant was incubated with the magnetic agarose beads containing the antibody overnight (Invitrogen, Dynabeads M-280 sheep anti-rabbit). Cells were washed twice with low salt wash buffer (50 mM Tris, 150 mM NaCl, 1 mM EDTA, 0.05% NP-40), and then were divided into two equal parts, one for detecting IP efficiency by western blotting. Another magnetic bead sample was added with 200 μl of DNA decrosslinking solution (10 mM Tris, 1Mm EDTA, 0.65% SDS), incubated at 65 °C for 16 h, and then proteinase K (20 mg/ml) was used to digest protein by incubating for 2 h at 37 °C. The DNA that bound to the cGAS protein was extracted through the mixture of phenol, chloroform, and isoamyl alcohol (25:24:1) (Thermo Fisher), and then was precipitated in 75% ethanol. Finally, the DNA was dissolved in the nuclease-free water and quantified by

Author Manuscript Author Manuscript Author Manuscript Author Manuscript

qPCR by using: Cytochrome c oxidase I (mtDNA gene) and housekeeping gene (18S rDNA) (27), the PCR primers used in the reaction are listed in Supplementary Table S1.

Mitochondrial DNA deletion and replenishment

For the analysis of how mtDNA manipulates Type I IFN responses, mitochondrial DNA (mtDNA) knockout and replenishment assay was performed by using Lip RNAiMAX Reagent and Pierce Protein Transfection Reagent Kit (Waltham, MA, USA) according to the manufacturer's instructions. Briefly, J744.1A macrophages were cultured to 80% density in RPMI 1640 medium supplemented with 10% FBS, and then were induced for 2 weeks to remove mtDNA by adding 1000 ng/ml Ethidium bromide, 25 μg/ml Uridine and 1 mM pyruvate (medium was changed once per day). To analyze whether mtDNA was completely knocked out, mtDNA copy numbers were determined by qPCR using primers for Cytochrome c oxidase I (mtDNA gene) and housekeeping gene (18S rDNA) (Fig. S4C). DNase I that was used to digest exogenously imported mtDNA was transfected into cells by using Pierce Protein Transfection Reagent Kit (89850, ThermoFisher) according to the manufacturer's instructions, and mtDNA, which was obtained from the cytosol by using DNeasy Blood & Tissue Kit according to the manufacturer's instructions, was replenished into J744.1A macrophages that had deleted mtDNA by using Lip RNAiMAX Reagent as previously described (28).

Bacterial burden assay

Animal blood was obtained by cardiac blood sampling on the sacrificed mouse, lung tissue was homogenized with PBS, BALF was obtained through alveolar lavage, and all samples were diluted to different gradients in PBS before being evenly distributed in LB dishes. The dishes were cultured in a 37°C incubator overnight, and the number of bacteria was counted. Each experiment was performed in triplicate.

Histological analysis

Lung tissues were fixed in 10% formalin (Sigma-Aldrich) for 48 h in 4 °C and then embedded in paraffin using a routine histologic procedure. H&E staining was carried out according to the standard staining procedure (26).

Flow cytometry

Bronchoalveolar lavage fluid (BALF) was obtained through alveolar lavage, blood samples were obtained through cardiac blood sampling, and erythrocytes were removed through the cell lysate. Lung tissues were homogenized with PBS and digested with collagenase. They were washed 3 times with PBS, then resuspended in 500 μl PBS. 200 μl of CD45, CD11b and MHCII antibody (BioLegend, San Diego, CA) with PBS (1:1000) were added to the groups of cells separately; $CD45^+/CD11b^+$ was used to mark myeloid progenitors, $CD11b^+/Gr1^+/MHCII^+$ was used to mark neutrophils. Cells were incubated in the dark for 30 minutes at room temperature, washed 2 times with PBS, and then resuspended in 1 ml PBS. The cells were filtered by using a 40 μm filter and were tested by flow cytometry (29).

Author Manuscript Author Manuscript Author Manuscript Author Manuscript

Quantification and statistical analysis

Data were presented as mean ± standard error means (SEM) determined from biological triplicates. Statistical analysis was performed with GraphPad (GraphPad Software, LaJolla, CA). Results in Figures 1, Figures 4A and Figure 5A were analyzed by Student's t-test compare with control group. Results in Figures 2A, 2B, 3E, Figures 3A, 3B, 3C, 3D, 3E, Figures 4B, Figures 5B, 5D, 5E, 5F and Figures 6B, 6D and 6E were analyzed by One Way ANOVA plus Tukey post hoc test; data in Figure 6A were analyzed by Kaplan-Meier Survival Analysis. Statistically significant differences are indicated as *$*p<0.05$, **$p<0.01$*.

Results

SU0268 potently inhibits the activity of OGG1 and decreases levels of pro-inflammatory cytokines in vitro

To determine the intrinsic cytotoxicity of SU0268 on mouse alveolar macrophage (MH-S) cells, we conducted MTT assays evaluating cell viability treated with different concentrations of the SU0268 (50, 25, 12.5, 6.25, 3.125, 1.5625, 0.78, 0.39 μM) for 24 hours. The data of Fig. 1A showed that SU0268 possessed some toxicity to MH-S cells with IC50 at 14.7 μM, and the toxicity is higher than in HEK293 and HeLa cell lines (15), which may be related to the different tolerance to inhibitors (SU0268) between human and mouse cell types. We further tested doses lower than IC50 to determine the optimal concentration for blocking OGG1 activity as 2 μM (Fig. 1B), which did not influence cell viability over an extended time (Fig. 1C). We thus chose 2 μM SU0268 for further study. To determine whether SU0268 can inhibit the activity of murine OGG1 from MH-S cells, we used a previously published fluorescence assay specific for OGG1 activity (23); the data showed when lysates were supplemented with SU0268 (1 μM), observed that OGG1 activity was dampened to ~15% relative to the DMSO control, the enzyme activity of OGG1 was strongly suppressed by SU0268 at 1 μM (Fig. 1D). Meanwhile, SU0268 also mildly inhibited the expression level of OGG1 by SU0268 at 2 μM for varied times (Fig. S1A, S1B). Further experiments carried out by incubating MH-S cells with SU0268 confirmed that the inhibitor increased levels of 8-oxo-dG in DNA, as expected after suppressed excision of this lesion (Fig. 1E, Fig. S1C).

Recent studies have demonstrated that inhibition of the expression of OGG1 can effectively inhibit the inflammatory response (7, 16). To further analyze the role of SU0268 as an anti-inflammatory agent in MH-S cells, the expression levels of pro-inflammatory cytokines TNF-α, IL-6 and IL-1β at different time points were evaluated using ELISA (Fig. 1F) and western blotting (Fig. 1G) after incubation with 2 μM SU0268 (MH-S cells can spontaneously produce inflammatory factors, albeit at much lower levels) (26, 30). Basal expression of inflammatory mediators was suppressed by SU0268, and the anti-inflammatory activity appeared to be strongest at 4 h and 8 h post treatment. Altogether, these data showed that SU0268 potently inhibits the activity of OGG1 and down-regulates levels of pro-inflammatory cytokines *in vitro*.

Author Manuscript Author Manuscript Author Manuscript Author Manuscript

SU0268 regulates innate inflammation through KRAS-ERK1-NF-κB axis

To further analyze the role of SU0268 in *P. aeruginosa* infection, the anti-inflammatory activity of SU0268 in PA14 infection was quantified by qPCR (Fig. 2A), ELISA (Fig. 2B) and western blotting (Fig. S2A). At rest, the NF-κB dimers are sequestered in the cytoplasm by binding with IκBs (κB inhibitors) (31). NF-κB is activated upon LPS or bacterial challenge, and is then freed to enter the nucleus to bind promoter regions of certain genes to initiate the inflammatory responses (32–34). Next, activation of NF-κB and the expression level of pro-inflammatory cytokines (TNF-α, IL-6) were evaluated by immunofluorescence (Fig. 2C, S2B). Furthermore, OGG1, as a DNA repair enzyme, initiates excessive inflammatory responses by activating the OGG1–BER-KRAS-ERK1/2-NF-κB circuit when bacterial infection induces DNA base lesions (7, 35, 36), the activation of KRAS is regulated by GEFs (37). Here we found that OGG1 regulation of inflammation is related to guanine nucleotide exchange factors (GEFs)/KRAS-ERK1-NF-κB axis, which were drastically down-regulated by SU0268 in cell culture (Fig. 2D). Together, these results indicate that SU0268 decreases innate inflammation by inhibiting the GEFs/KRAS-ERK1-NF-κB axis upon *P. aeruginosa* infection.

OGG1 inhibitor regulates the release of mtDNA

ROS production has been linked to various cellular signaling pathways (38). The expression levels of ROS are documented to increase upon exposure to bacterial infection (39). Increased ROS-induced DNA damage can be repaired by OGG1 through the DNA base excision repair pathway (OGG1–BER) (40). However, the levels of ROS-induced DNA damage have not been decreased instead of increasing by generating repair intermediates (41). To investigate the impact of ROS on DNA damage during *P. aeruginosa* infection, the amount of ROS released was measured using NBT (Fig. 3A) and H_2DCF assay (Fig. 3B, S3A). Concomitantly, the degree of DNA damage was assessed by the comet assay (Fig. 3C), and results demonstrate increased ROS and DNA damage in MH-S cells by *P. aeruginosa*. Significantly, treatment with SU0268 attenuated DNA damage compared with *P. aeruginosa* infection, which is consistent with lowered levels of base excision and decreased levels of DNA strand cleavage. Mitochondria play an important role in regulating the innate immune response to infection and DNA damage (42). The accumulation of DNA damage initiates mitochondrial dysfunction (43). To investigate the role of mitochondria in the regulation of *P. aeruginosa* infection, we examined mitochondrial potential using the JC-1 fluorescence assay and found that SU0268 significantly restored the infection-mediated mitochondrial potential (Fig. 3D, S3B). Mitochondrial DNA (mtDNA) is critical for maintaining sufficient cellular energy required for cell development and function, in addition to regulating a variety of immune responses (44). Mitochondrial DNA maintenance defects (MDMDs), which are caused by mitochondrial DNA synthesis disorders will further trigger insufficient mtDNA-encoded protein synthesis and energy production resulting in organ dysfunction (45, 46). We used qPCR (Fig. 3E) and immunofluorescence (Fig. S3C) to detect released mtDNA that was increased upon *P. aeruginosa* infection and further augmented by incubation with SU0268. Collectively, these observations strongly imply that this OGG1 inhibitor regulates the mitochondrial immune response by regulating the release of mtDNA.

Author Manuscript Author Manuscript Author Manuscript Author Manuscript

OGG1 inhibitor facilitates mtDNA release by manipulating BAK/BAK macropores-induced apoptosis

To further characterize the critical role of an OGG1 inhibitor in modulating the mitochondrial immune response by regulating the release of mtDNA in *P. aeruginosa* infection, a qPCR microarray was executed to screen 60 genes involved in mtDNA release and mitochondrial function after treatment with SU0268 for 8 hours, then infection with PA14 for 2 hours, PA14 infection group without SU0268 as control (Fig. 4A) (Gene primers are shown in Supplementary Table S2). We found that the expression of *Bak* and *Bax* was significantly increased. Bak/Bax, as a pro-apoptotic factor, mediate cell clearance programming and tissue homeostasis to prevent a potentially damaging inflammatory or immune response (24). We hypothesized that BAK/BAX may receive a signal from apoptotic mitochondria, which may be associated with DNA damage. We found that cell apoptosis was increased by the OGG1 inhibitor SU0268 (Fig. 4B). Meanwhile, cytochrome c loss has also been shown to manipulate the release of mtDNA by mitochondrial apoptosis (24, 47). To firmly determine whether increased the release of mtDNA is associated with mitochondrial apoptosis, immunofluorescence and western blotting were also performed to detect released cytochrome c from mitochondria. We found that cytochrome c loss was significantly increased following infection and could be further increased by the OGG1 inhibitor (Fig. 4C). These results together suggest that the OGG1 inhibitor facilitates mtDNA release by modulating BAK/BAX macropore-induced apoptosis.

Increased release of mtDNA activates the cGAS-TBK-IRF3-IFN-β pathway by increasing binding with cGAS to influence type I IFN responses

Research has shown that *Ogg1* knock out mice increased oxidized mtDNA in macrophages (48). It remains unknown how mtDNA participates in immune regulation during *P. aeruginosa* infection. To gain further insights into the role of mtDNA in regulating inflammatory response, we utilized RT^2 Profiler PCR Cancer Inflammation & Immunity Crosstalk array to identify key regulatory genes (330231 PAMM-181Z, QIAGEN, USA) (Figure 5A). The results show that the signal transducer and activator of transcription 1 (*Stat1*) were highly activated. Tyrosine kinase 2 (TYK2) and Janus kinase 1 (JAK1) enable the phosphorylation of STAT1/STAT2, which activates the transactivation of multiple genes, including cGAS (GMP-AMP synthase) (49). It has been widely reported that mitochondrial DNA facilitates the activation of the cGAS-TBK-IRF3 circuit (50). We hypothesized that elevated released mtDNA activates the cGAS pathway upon *P. aeruginosa* infection. Therefore, the cGAS signaling pathway proteins were measured by western blotting (Figure. 5B), and nuclear transfer of IRF3 was also augmented as detected by immunofluorescence (Figure. S4A). To clarify the mechanism of the mtDNA-driven cGAS pathway, colocalization of mtDNA and cGAS was revealed by immunofluorescence (Figure. 5C). Next, a cGAS antibody was used to pull-down mtDNA under different processing conditions using immunoprecipitation (IP) assay, and mtDNA was co-precipitated by cGAS antibodies, which was quantified by qPCR (Figure. 5D). These data strongly support that increased release of mtDNA activated the cGAS pathway by increasing binding to cGAS. Activation of the cGAS pathway is critical for the generation of Type I interferons (IFN) (51). Certainly, IFN is essential for host defense against bacterial infection by modulating innate immune responses (52). Mice exhibited significantly improved clearance of *P. aeruginosa*

Author Manuscript Author Manuscript Author Manuscript Author Manuscript

after being pretreated with the activator of IFN-β (53). Next, we examined the release of IFNβ in MH-S and J744.1A cells by ELISA (Figure. 5E, 5F), and the results revealed that the OGG1 inhibitor elicited increased expression of IFNβ. Notably, this situation was reversed after knocking down cGAS with small interfering RNA (Figure. 5E); the cGAS knockdown efficiency was detected by western blotting after 48 h transfection (Figure. S4B). Meanwhile, to further confirm that mtDNA regulation the release of IFNβ is through cGAS related signal pathway, mitochondrial DNA deletion and replenishment assays were performed in J744.1A macrophages without mtDNA (Fig. S4C, detailed in materials and methods); the results revealed that replenishment mtDNA increased expression of IFNβ. However, there is no significant difference when knocking down cGAS with small interfering RNA (Figure. 5F). These results strongly suggest that mtDNA regulation of the Type I IFN responses was through the cGAS signaling pathway. Consistently, these experiments demonstrate that increased release of mtDNA activates the cGAS-TBK-IRF3-IFNβ pathway by increasing binding with cGAS to manipulate Type I IFN responses.

Small-molecule inhibitor of OGG1 significantly inhibits inflammatory responses and mitigates *P. aeruginosa* infection

To gain deep insights into the role of OGG1 inhibitor mediated inflammatory and mtDNA-mediated Type I IFN responses in *P. aeruginosa* infection *in vivo* in parallel with *in vitro*, we performed a survival curve to explore the prevention and therapeutic effects of SU0268 in MH-S cells and C57BL/6N mice. The results showed that pretreatment with SU0268 increased survival rates compared to controls without SU0268 pretreatment in MH-S cells and C57BL/6N mice (Fig. 6A, S5A). Moreover, SU0268 also showed therapeutic activity after the MH-S cells and animals were infected by the PA14 bacterium (Fig. S5B, S5C). In a separate study, mouse pharmacokinetic data for SU0268 showed half-life ($t_{1/2}$) approximately 4.0 +/− 0.7 hours as performed Absorption Systems Inc. Next, bacterial burdens were quantified by colony-forming units (CFU) in the lung, blood and BALF (Fig. 6B and S5D), which showed that the burden of PA14 was significantly decreased in the mice treated with SU0268. Furthermore, we also found significant improvement in lung tissue damage in mice by immunohistochemistry staining (Fig. 6C) and significantly decreased expression levels of TNF-α, IL-6 and IL-1β in the presence of the inhibitor (Fig. S5E). Conversely, the expression level of IFN-β was up-regulated in the mouse primary BMDM cells after treatment with SU0268 for 8 hours, followed by infection with PA14 for 2 hours (Fig. 6D). Neutrophils play essential roles in the clearance of bacteria and viruses (54). However, excessive recruitment of neutrophils significantly aggravates the injury of lung tissue (55, 56). Next, we examined the number of neutrophils in mouse BALF, blood and lung by staining with $CD11b^+/Gr1^+/MHCII^+$ antibodies via flow cytometry (Fig. 6E). We found the myeloid progenitor cells ($CD45^+/CD11b^+$) and neutrophils ($CD11b^+/Gr1^+/MHCII^+$) to be significantly increased in PA14 infection, but significantly decreased with prior treatment of SU0268. Consistent with previous observations, this result supports the conclusion that the small-molecule OGG1 inhibitor regulates inflammatory response and mtDNA-mediated Type I IFN release to mitigate bacterial infection during *P. aeruginosa* infection *in vivo* and *in vitro*, as shown in Figure 7.

Author Manuscript Author Manuscript Author Manuscript Author Manuscript

Discussion

In this study, we investigated the role of the OGG-1 inhibitor SU0268 in *P. aeruginosa* infection, which showed that pharmacological inhibition of OGG1 in place of a knockout strategy decreased the expression of pro-inflammatory factors, allowing the approach to be applicable in clinical scenarios. Importantly, our data elaborated a new mechanism whereby a small-molecule OGG1 inhibitor decreases inflammatory and mtDNA-mediated Type I IFN responses to inhibit bacterial spread and improve susceptibility after *P. aeruginosa* infection. Our research provides theoretical support for a small-molecule inhibitor as a potential anti-infective drug to decrease bacterially-induced inflammation.

Stimulation of the external environment, such as bacterial or viral infections, will result in dysregulation of ROS generation, which will cause DNA damage (57). OGG1, which acts as a base excision DNA repair (BER) enzyme, is crucial for modulation of the coordination between innate and adaptive immunity through regulating oxidative stress and immune responses (58). In the BER pathway, OGG1 binds to 8-oxoG adducts to form an OGG1/8-oxoG complex, which functions as a prototypic guanine nucleotide exchange factor (GEF) (59). The Rho family of GTPases, a subfamily of the Ras superfamily, controls multiple cellular processes, including gene expression, microtubule dynamics and membrane transport, and are activated by GEFs (60–62). It has previously been reported that OGG1 increased activation of Rho-GTPase in oxidatively-stressed cells (63). GEF-H1 (a RhoA activator, as a GEF for the Rho small GTPase proteins) has been well documented to act as an integrator of microtubule and actin dynamics in diverse cell functions (64). GEF-H1 is also shown to promote RAS-driven MAPK via modulating KSR-1 phosphorylation (65). OGG1 initiates inflammatory responses by activating the OGG1/KRAS/NF-κB pathway during bacterial infection or ROS-induced DNA damage (7, 41). Our data demonstrate that SU0268 decreases the inflammatory responses through the GEFs/KRAS-ERK1-NF-κB axis, which may be related to decreased OGG1-BER activity and thereby down-regulating GEFs expression. This will inhibit Ras activation by regulating the exchange of guanosine diphosphate (GDP) to guanosine triphosphate (GTP) and decreasing expression of pro-inflammatory genes and innate immune responses (66). The extent of bacterial replication may be influenced by host antibacterial immune responses, including inflammatory responses (67). Meanwhile, anti-inflammatory reaction can suppress the growth of bacteria and reduce the burden of pathogenic damage during infection (9, 68). Together, our data showed that OGG1 inhibitor SU0268 decreased the inflammatory response through the GEFs/KRAS-ERK1-NF-κB axis, which may help mitigate *P. aeruginosa* infection.

The mouse strains lacking *Ogg1* (*Ogg1*$^{-/-}$) or *Nth1 (Nth1*$^{-/-}$) have been reported to have an increase in the copy numbers of mtDNA, which may be related to the decrease in the repair function of OGG1 (69). Mitochondrial DNA (mtDNA) is a small circular double-stranded DNA that localizes in the mitochondrial matrix. mtDNA functions as a signaling platform to facilitate antibacterial immunity and regulating anti-microbial signaling by activating different kinds of molecular pathways upon exposure to bacteria or viruses (59, 61, 62). mtDNA is released into the cytoplasm through BAK and BAX-mediated mitochondrial apoptosis, where it can be recognized by DNA sensor cGAS and incite innate immunity responses through the cGAS/STING signaling (63), increasing type I interferon secretion

Author Manuscript Author Manuscript Author Manuscript Author Manuscript

(42). Our study demonstrated that OGG1 inhibitor (SU0268) increased the release of mtDNA into the cytoplasm, where activates the cGAS-TBK-IRF3-IFNβ circuit and triggers Type I IFN responses.

Type I interferons as pleiotropic cytokines are essential for host defense against viral and bacterial infection by modulating innate and adaptive immune responses (70), which can be activated by the cGAS/TBK/IRF3 signaling pathway (71, 72). Activated type I IFNs play a decisive role in the inhibition of bacterial replication and regulation of anti-inflammatory responses to protect against tissue-damage-induced mortality (51). Mechanistically, Type I IFN inhibits the acute phase expression of TNFα and IL-1β cytokines by upregulating the anti-inflammatory cytokine expression of IL-10 and IL-27 (73). IFNAR1- or NOD1-deficient mice that cannot induce the expression of type I IFN in an IRF7-dependent manner fail to restrict *H. pylori* proliferation and aggravated lung injury (74). Our analysis revealed that increased IFNβ secretion by mtDNA/cGAS/TBK/IRF3 axis mitigates *P. aeruginosa* infection. Together, our data illustrated that the OGG1 inhibitor SU0268 may regulate inflammatory responses to attenuate *P. aeruginosa* infection by activating mitochondrial immune response through a mtDNA/cGAS/TBK/IRF3/ IFNβ axis. Other acute clinical lung infections are also exacerbated by an induced inflammatory response. For example, patients with confirmed coronavirus disease (COVID-19) show elevated levels of cytokines including IL-6, and it has been proposed that agents that lower IL-6 signaling may be an effective therapeutic approach (75, 76). Given that SU0268 inhibits with a short half-life in mice (4 h) IL-6 expression and inflammatory responses in *P. aeruginosa* infection, it suggests that further studies of this compound in models of viral lung infections such as those caused by SARS-CoV-2 may also be warranted.

In summary, we have investigated the role of OGG1 inhibitor SU0268 in *P. aeruginosa* infection, which shows significant inhibition of inflammatory responses and mitigates *P. aeruginosa* (PA14) infection. Mechanistically, the small-molecule inhibitor of OGG1 orchestrates inflammatory and mtDNA-mediated Type I IFN responses to regulate anti-inflammatory responses and attenuates bacterial infection by inhibiting the activity of OGG1 in excision of 8-oxoG and activating the mtDNA-cGAS-TBK-IRF3-IFNβ circuit. These results indicate that OGG1 may indirectly regulate the expression of IFNβ to mediate adaptive immunity, which provides novel insights for the future development of OGG1 inhibitors to treat bacterial infection.

Supplementary Material

Refer to Web version on PubMed Central for supplementary material.

Acknowledgements

Immunofluorescent, Histological and Flow Cytometry images were captured at the UND Imaging Core and Flow Cytometry Core with assistance from Dr. Abrahamson, Dr. DeMontigny and Dr. Adkins.

This work was supported by National Institutes of Health Grants R01 AI109317-01A1, R01 AI138203, P20 GM113123 and AI097532-01A1 to MW, and grant CA217809 to ETK. The UND Imaging Core and Flow Cytometry Core were supported by NIH P20 GM113123 and P20 GM103442, respectively. The funders had no role in study design, data collection and analysis, decision to publish, or preparation of the manuscript.

Author Manuscript Author Manuscript Author Manuscript Author Manuscript

References

1. Hoggarth A, Weaver A, Pu Q, Huang T, Schettler J, Chen F, Yuan X, and Wu M. 2019 Mechanistic research holds promise for bacterial vaccines and phage therapies for Pseudomonas aeruginosa. Drug design, development and therapy 13: 909–924.
2. Zhang Y, Zhou CM, Pu Q, Wu Q, Tan S, Shao X, Zhang W, Xie Y, Li R, Yu XJ, Wang R, Zhang L, Wu M, and Deng X. 2019 Pseudomonas aeruginosa Regulatory Protein AnvM Controls Pathogenicity in Anaerobic Environments and Impacts Host Defense. mBio 10: e01362–01319. [PubMed: 31337721]
3. Li R, Fang L, Pu Q, Lin P, Hoggarth A, Huang H, Li X, Li G, and Wu M. 2016 Lyn prevents aberrant inflammatory responses to Pseudomonas infection in mammalian systems by repressing a SHIP-1-associated signaling cluster. Signal transduction and targeted therapy 1: 16032. [PubMed: 29263906]
4. Pu Q, Gan C, Li R, Li Y, Tan S, Li X, Wei Y, Lan L, Deng X, Liang H, Ma F, and Wu M. 2017 Atg7 Deficiency Intensifies Inflammasome Activation and Pyroptosis in Pseudomonas Sepsis. Journal of immunology 198: 3205–3213.
5. Pan L, Hao W, Zheng X, Zeng X, Ahmed Abbasi A, Boldogh I, and Ba X. 2017 OGG1-DNA interactions facilitate NF-kappaB binding to DNA targets. Scientific reports 7: 43297. [PubMed: 28266569]
6. Li X, He S, Li R, Zhou X, Zhang S, Yu M, Ye Y, Wang Y, Huang C, and Wu M. 2016 Pseudomonas aeruginosa infection augments inflammation through miR-301b repression of c-Myb-mediated immune activation and infiltration. Nature microbiology 1: 16132.
7. Aguilera-Aguirre L, Bacsi A, Radak Z, Hazra TK, Mitra S, Sur S, Brasier AR, Ba X, and Boldogh I. 2014 Innate inflammation induced by the 8-oxoguanine DNA glycosylase-1-KRAS-NF-kappaB pathway. Journal of immunology 193: 4643–4653.
8. Ba X, Bacsi A, Luo J, Aguilera-Aguirre L, Zeng X, Radak Z, Brasier AR, and Boldogh I. 2014 8-oxoguanine DNA glycosylase-1 augments proinflammatory gene expression by facilitating the recruitment of site-specific transcription factors. Journal of immunology 192: 2384–2394.
9. Touati E, Michel V, Thiberge JM, Ave P, Huerre M, Bourgade F, Klungland A, and Labigne A. 2006 Deficiency in OGG1 protects against inflammation and mutagenic effects associated with H. pylori infection in mouse. Helicobacter 11: 494–505. [PubMed: 16961812]
10. Bacsi A, Chodaczek G, Hazra TK, Konkel D, and Boldogh I. 2007 Increased ROS generation in subsets of OGG1 knockout fibroblast cells. Mechanisms of ageing and development 128: 637–649. [PubMed: 18006041]
11. Li G, Yuan K, Yan C, Fox J 3rd, Gaid M, Breitwieser W, Bansal AK, Zeng H, Gao H, and Wu M. 2012 8-Oxoguanine-DNA glycosylase 1 deficiency modifies allergic airway inflammation by regulating STAT6 and IL-4 in cells and in mice. Free radical biology & medicine 52: 392–401. [PubMed: 22100973]
12. Mabley JG, Pacher P, Deb A, Wallace R, Elder RH, and Szabo C. 2005 Potential role for 8-oxoguanine DNA glycosylase in regulating inflammation. FASEB journal : official publication of the Federation of American Societies for Experimental Biology 19: 290–292. [PubMed: 15677345]
13. Kumagae Y, Hirahashi M, Takizawa K, Yamamoto H, Gushima M, Esaki M, Matsumoto T, Nakamura M, Kitazono T, and Oda Y. 2018 Overexpression of MTH1 and OGG1 proteins in ulcerative colitis-associated carcinogenesis. Oncology letters 16: 1765–1776. [PubMed: 30008864]
14. Donley N, Jaruga P, Coskun E, Dizdaroglu M, McCullough AK, and Lloyd RS. 2015 Small Molecule Inhibitors of 8-Oxoguanine DNA Glycosylase-1 (OGG1). ACS chemical biology 10: 2334–2343. [PubMed: 26218629]
15. Tahara YK, Auld D, Ji D, Beharry AA, Kietrys AM, Wilson DL, Jimenez M, King D, Nguyen Z, and Kool ET. 2018 Potent and Selective Inhibitors of 8-Oxoguanine DNA Glycosylase. Journal of the American Chemical Society 140: 2105–2114. [PubMed: 29376367]
16. Visnes T, Cazares-Korner A, Hao W, Wallner O, Masuyer G, Loseva O, Mortusewicz O, Wiita E, Sarno A, Manoilov A, Astorga-Wells J, Jemth AS, Pan L, Sanjiv K, Karsten S, Gokturk C, Grube

Author Manuscript Author Manuscript Author Manuscript Author Manuscript

M, Homan EJ, Hanna BMF, Paulin CBJ, Pham T, Rasti A, Berglund UW, von Nicolai C, Benitez-Buelga C, Koolmeister T, Ivanic D, Iliev P, Scobie M, Krokan HE, Baranczewski P, Artursson P, Altun M, Jensen AJ, Kalderen C, Ba X, Zubarev RA, Stenmark P, Boldogh I, and Helleday T. 2018 Small-molecule inhibitor of OGG1 suppresses proinflammatory gene expression and inflammation. Science 362: 834–839. [PubMed: 30442810]

17. Chen Y, Zhou Z, and Min W. 2018 Mitochondria, Oxidative Stress and Innate Immunity. Frontiers in physiology 9: 1487. [PubMed: 30405440]
18. Ablasser A, and Chen ZJ. 2019 cGAS in action: Expanding roles in immunity and inflammation. Science 363: eaat8657. [PubMed: 30846571]
19. Motwani M, Pesiridis S, and Fitzgerald KA. 2019 DNA sensing by the cGAS-STING pathway in health and disease. Nature reviews. Genetics 20: 657–674.
20. Lahaye X, Gentili M, Silvin A, Conrad C, Picard L, Jouve M, Zueva E, Maurin M, Nadalin F, Knott GJ, Zhao B, Du F, Rio M, Amiel J, Fox AH, Li P, Etienne L, Bond CS, Colleaux L, and Manel N. 2018 NONO Detects the Nuclear HIV Capsid to Promote cGAS-Mediated Innate Immune Activation. Cell 175: 488–501. [PubMed: 30270045]
21. Li R, Tan S, Yu M, Jundt MC, Zhang S, and Wu M. 2015 Annexin A2 Regulates Autophagy in Pseudomonas aeruginosa Infection through the Akt1-mTOR-ULK1/2 Signaling Pathway. Journal of immunology 195: 3901–3911.
22. Li X, He S, Zhou X, Ye Y, Tan S, Zhang S, Li R, Yu M, Jundt MC, Hidebrand A, Wang Y, Li G, Huang C, and Wu M. 2016 Lyn Delivers Bacteria to Lysosomes for Eradication through TLR2-Initiated Autophagy Related Phagocytosis. PLoS pathogens 12: e1005363. [PubMed: 26735693]
23. Wilson DL, and Kool ET. 2019 Ultrafast Oxime Formation Enables Efficient Fluorescence Light-up Measurement of DNA Base Excision. Journal of the American Chemical Society 141: 19379–19388. [PubMed: 31774658]
24. McArthur K, Whitehead LW, Heddleston JM, Li L, Padman BS, Oorschot V, Geoghegan ND, Chappaz S, Davidson S, San Chin H, Lane RM, Dramicanin M, Saunders TL, Sugiana C, Lessene R, Osellame LD, Chew TL, Dewson G, Lazarou M, Ramm G, Lessene G, Ryan MT, Rogers KL, van Delft MF, and Kile BT. 2018 BAK/BAX macropores facilitate mitochondrial herniation and mtDNA efflux during apoptosis. Science 359: eaao6047. [PubMed: 29472455]
25. Sivandzade F, Bhalerao A, and Cucullo L. 2019 Analysis of the Mitochondrial Membrane Potential Using the Cationic JC-1 Dye as a Sensitive Fluorescent Probe. Bio-protocol 9: e3128. [PubMed: 30687773]
26. Wu Q, Wang B, Zhou C, Lin P, Qin S, Gao P, Wang Z, Xia Z, and Wu M. 2019 Bacterial Type I CRISPR-Cas systems influence inflammasome activation in mammalian host by promoting autophagy. Immunology 158: 240–251. [PubMed: 31429483]
27. Bronner DN, and O'Riordan MX. 2016 Measurement of Mitochondrial DNA Release in Response to ER Stress. Bio-protocol 6: e1839. [PubMed: 31106234]
28. Jabir MS, Hopkins L, Ritchie ND, Ullah I, Bayes HK, Li D, Tourlomousis P, Lupton A, Puleston D, Simon AK, Bryant C, and Evans TJ. 2015 Mitochondrial damage contributes to Pseudomonas aeruginosa activation of the inflammasome and is downregulated by autophagy. Autophagy 11: 166–182. [PubMed: 25700738]
29. Wang Z, Pu Q, Lin P, Li C, Jiang J, and Wu M. 2019 Design of Cecal Ligation and Puncture and Intranasal Infection Dual Model of Sepsis-Induced Immunosuppression. Journal of visualized experiments : JoVE: 10.3791/59386.
30. Li R, Fang L, Pu Q, Bu H, Zhu P, Chen Z, Yu M, Li X, Weiland T, Bansal A, Ye SQ, Wei Y, Jiang J, and Wu M. 2018 MEG3–4 is a miRNA decoy that regulates IL-1beta abundance to initiate and then limit inflammation to prevent sepsis during lung infection. Science signaling 11: eaao2387. [PubMed: 29945883]
31. Leibowitz SM, and Yan J. 2016 NF-kappaB Pathways in the Pathogenesis of Multiple Sclerosis and the Therapeutic Implications. Frontiers in molecular neuroscience 9: 84. [PubMed: 27695399]
32. Bryant CE, Spring DR, Gangloff M, and Gay NJ. 2010 The molecular basis of the host response to lipopolysaccharide. Nature reviews. Microbiology 8: 8–14.
33. Oeckinghaus A, and Ghosh S. 2009 The NF-kappaB family of transcription factors and its regulation. Cold Spring Harbor perspectives in biology 1: a000034. [PubMed: 20066092]

Author Manuscript Author Manuscript Author Manuscript Author Manuscript

34. Camargo RG, Riccardi DM, Ribeiro HQ, Carnevali LC Jr., de Matos-Neto EM, Enjiu L, Neves RX, Lima JD, Figueredo RG, de Alcantara PS, Maximiano L, Otoch J, Batista M Jr., Puschel G, and Seelaender M. 2015 NF-kappaBp65 and Expression of Its Pro-Inflammatory Target Genes Are Upregulated in the Subcutaneous Adipose Tissue of Cachectic Cancer Patients. Nutrients 7: 4465–4479. [PubMed: 26053616]
35. Boldogh I, Hajas G, Aguilera-Aguirre L, Hegde ML, Radak Z, Bacsi A, Sur S, Hazra TK, and Mitra S. 2012 Activation of ras signaling pathway by 8-oxoguanine DNA glycosylase bound to its excision product, 8-oxoguanine. The Journal of biological chemistry 287: 20769–20773. [PubMed: 22568941]
36. German P, Szaniszlo P, Hajas G, Radak Z, Bacsi A, Hazra TK, Hegde ML, Ba X, and Boldogh I. 2013 Activation of cellular signaling by 8-oxoguanine DNA glycosylase-1-initiated DNA base excision repair. DNA repair 12: 856–863. [PubMed: 23890570]
37. Liu P, Wang Y, and Li X. 2019 Targeting the untargetable KRAS in cancer therapy. Acta pharmaceutica Sinica. B 9: 871–879. [PubMed: 31649840]
38. Zorov DB, Juhaszova M, and Sollott SJ. 2014 Mitochondrial reactive oxygen species (ROS) and ROS-induced ROS release. Physiological reviews 94: 909–950. [PubMed: 24987008]
39. Liu J, Chen X, Dou M, He H, Ju M, Ji S, Zhou J, Chen C, Zhang D, Miao C, and Song Y. 2019 Particulate matter disrupts airway epithelial barrier via oxidative stress to promote Pseudomonas aeruginosa infection. Journal of thoracic disease 11: 2617–2627. [PubMed: 31372298]
40. Li PY, Chang YC, Tzang BS, Chen CC, and Liu YC. 2007 Antibiotic amoxicillin induces DNA lesions in mammalian cells possibly via the reactive oxygen species. Mutation research 629: 133–139. [PubMed: 17382580]
41. Wang R, Li C, Qiao P, Xue Y, Zheng X, Chen H, Zeng X, Liu W, Boldogh I, and Ba X. 2018 OGG1-initiated base excision repair exacerbates oxidative stress-induced parthanatos. Cell death & disease 9: 628. [PubMed: 29795387]
42. Rongvaux A 2018 Innate immunity and tolerance toward mitochondria. Mitochondrion 41: 14–20. [PubMed: 29054471]
43. Saki M, and Prakash A. 2017 DNA damage related crosstalk between the nucleus and mitochondria. Free radical biology & medicine 107: 216–227. [PubMed: 27915046]
44. Stein A, and Sia EA. 2017 Mitochondrial DNA repair and damage tolerance. Frontiers in bioscience 22: 920–943.
45. El-Hattab AW, Craigen WJ, and Scaglia F. 2017 Mitochondrial DNA maintenance defects. Biochimica et biophysica acta. Molecular basis of disease 1863: 1539–1555. [PubMed: 28215579]
46. El-Hattab AW, and Scaglia F. 2013 Mitochondrial DNA depletion syndromes: review and updates of genetic basis, manifestations, and therapeutic options. Neurotherapeutics : the journal of the American Society for Experimental NeuroTherapeutics 10: 186–198. [PubMed: 23385875]
47. Zhang M, Zheng J, Nussinov R, and Ma B. 2017 Release of Cytochrome C from Bax Pores at the Mitochondrial Membrane. Scientific reports 7: 2635. [PubMed: 28572603]
48. Tumurkhuu G, Shimada K, Dagvadorj J, Crother TR, Zhang W, Luthringer D, Gottlieb RA, Chen S, and Arditi M. 2016 Ogg1-Dependent DNA Repair Regulates NLRP3 Inflammasome and Prevents Atherosclerosis. Circulation research 119: e76–90. [PubMed: 27384322]
49. Galluzzi L, Vanpouille-Box C, Bakhoum SF, and Demaria S. 2018 SnapShot: CGAS-STING Signaling. Cell 173: 276–276.e271. [PubMed: 29570996]
50. Liu S, Feng M, and Guan W. 2016 Mitochondrial DNA sensing by STING signaling participates in inflammation, cancer and beyond. International journal of cancer 139: 736–741. [PubMed: 26939583]
51. Boxx GM, and Cheng G. 2016 The Roles of Type I Interferon in Bacterial Infection. Cell host & microbe 19: 760–769. [PubMed: 27281568]
52. McNab F, Mayer-Barber K, Sher A, Wack A, and O'Garra A. 2015 Type I interferons in infectious disease. Nature reviews. Immunology 15: 87–103.
53. Parker D, Cohen TS, Alhede M, Harfenist BS, Martin FJ, and Prince A. 2012 Induction of type I interferon signaling by Pseudomonas aeruginosa is diminished in cystic fibrosis epithelial cells. American journal of respiratory cell and molecular biology 46: 6–13. [PubMed: 21778412]

Author Manuscript Author Manuscript Author Manuscript Author Manuscript

54. Wang J, Hossain M, Thanabalasuriar A, Gunzer M, Meininger C, and Kubes P. 2017 Visualizing the function and fate of neutrophils in sterile injury and repair. Science 358: 111–116. [PubMed: 28983053]
55. Chen GY, and Nunez G. 2010 Sterile inflammation: sensing and reacting to damage. Nature reviews. Immunology 10: 826–837.
56. Wright HL, Moots RJ, Bucknall RC, and Edwards SW. 2010 Neutrophil function in inflammation and inflammatory diseases. Rheumatology 49: 1618–1631. [PubMed: 20338884]
57. Barzilai A, and Yamamoto K. 2004 DNA damage responses to oxidative stress. DNA repair 3: 1109–1115. [PubMed: 15279799]
58. Pazmandi K, Suto M, Fekete T, Varga A, Boldizsar E, Boldogh I, and Bacsi A. 2019 Oxidized base 8-oxoguanine, a product of DNA repair processes, contributes to dendritic cell activation. Free radical biology & medicine 143: 209–220. [PubMed: 31408726]
59. Hajas G, Bacsi A, Aguilera-Aguirre L, Hegde ML, Tapas KH, Sur S, Radak Z, Ba X, and Boldogh I. 2013 8-Oxoguanine DNA glycosylase-1 links DNA repair to cellular signaling via the activation of the small GTPase Rac1. Free radical biology & medicine 61: 384–394. [PubMed: 23612479]
60. Scheffzek K, Ahmadian MR, Kabsch W, Wiesmuller L, Lautwein A, Schmitz F, and Wittinghofer A. 1997 The Ras-RasGAP complex: structural basis for GTPase activation and its loss in oncogenic Ras mutants. Science 277: 333–338. [PubMed: 9219684]
61. Voena C, and Chiarle R. 2019 RHO Family GTPases in the Biology of Lymphoma. Cells 8: 646–662.
62. Buchsbaum RJ 2007 Rho activation at a glance. Journal of cell science 120: 1149–1152. [PubMed: 17376960]
63. Luo J, Hosoki K, Bacsi A, Radak Z, Hegde ML, Sur S, Hazra TK, Brasier AR, Ba X, and Boldogh I. 2014 8-Oxoguanine DNA glycosylase-1-mediated DNA repair is associated with Rho GTPase activation and alpha-smooth muscle actin polymerization. Free radical biology & medicine 73: 430–438. [PubMed: 24681335]
64. Ren Y, Li R, Zheng Y, and Busch H. 1998 Cloning and characterization of GEF-H1, a microtubule-associated guanine nucleotide exchange factor for Rac and Rho GTPases. The Journal of biological chemistry 273: 34954–34960. [PubMed: 9857026]
65. Cullis J, Meiri D, Sandi MJ, Radulovich N, Kent OA, Medrano M, Mokady D, Normand J, Larose J, Marcotte R, Marshall CB, Ikura M, Ketela T, Moffat J, Neel BG, Gingras AC, Tsao MS, and Rottapel R. 2014 The RhoGEF GEF-H1 is required for oncogenic RAS signaling via KSR-1. Cancer cell 25: 181–195. [PubMed: 24525234]
66. Bacsi A, Aguilera-Aguirre L, Szczesny B, Radak Z, Hazra TK, Sur S, Ba X, and Boldogh I. 2013 Down-regulation of 8-oxoguanine DNA glycosylase 1 expression in the airway epithelium ameliorates allergic lung inflammation. DNA repair 12: 18–26. [PubMed: 23127499]
67. Yuk JM, Yoshimori T, and Jo EK. 2012 Autophagy and bacterial infectious diseases. Experimental & molecular medicine 44: 99–108. [PubMed: 22257885]
68. Shirin H, Moss SF, Kancherla S, Kancherla K, Holt PR, Weinstein IB, and Sordillo EM. 2006 Non-steroidal anti-inflammatory drugs have bacteriostatic and bactericidal activity against Helicobacter pylori. Journal of gastroenterology and hepatology 21: 1388–1393. [PubMed: 16911681]
69. Chimienti G, Pesce V, Fracasso F, Russo F, de Souza-Pinto NC, Bohr VA, and Lezza AMS. 2019 Deletion of OGG1 Results in a Differential Signature of Oxidized Purine Base Damage in mtDNA Regions. International journal of molecular sciences 20: 3302.
70. Ivashkiv LB, and Donlin LT. 2014 Regulation of type I interferon responses. Nature reviews. Immunology 14: 36–49.
71. Ishikawa H, and Barber GN. 2008 STING is an endoplasmic reticulum adaptor that facilitates innate immune signalling. Nature 455: 674–678. [PubMed: 18724357]
72. Sun L, Wu J, Du F, Chen X, and Chen ZJ. 2013 Cyclic GMP-AMP synthase is a cytosolic DNA sensor that activates the type I interferon pathway. Science 339: 786–791. [PubMed: 23258413]
73. Iyer SS, Ghaffari AA, and Cheng G. 2010 Lipopolysaccharide-mediated IL-10 transcriptional regulation requires sequential induction of type I IFNs and IL-27 in macrophages. Journal of immunology 185: 6599–6607.

Author Manuscript Author Manuscript Author Manuscript Author Manuscript

74. Watanabe T, Asano N, Fichtner-Feigl S, Gorelick PL, Tsuji Y, Matsumoto Y, Chiba T, Fuss IJ, Kitani A, and Strober W. 2010 NOD1 contributes to mouse host defense against Helicobacter pylori via induction of type I IFN and activation of the ISGF3 signaling pathway. The Journal of clinical investigation 120: 1645–1662. [PubMed: 20389019]

75. McGonagle D, Sharif K, O'Regan A, and Bridgewood C. 2020 The Role of Cytokines including Interleukin-6 in COVID-19 induced Pneumonia and Macrophage Activation Syndrome-Like Disease. Autoimmunity reviews 19: 102537. [PubMed: 32251717]

76. Ma J, Xia P, Zhou Y, Liu Z, Zhou X, Wang J, Li T, Yan X, Chen L, Zhang S, Qin Y, and Li X. 2020 Potential effect of blood purification therapy in reducing cytokine storm as a late complication of critically ill COVID-19. Clinical immunology 214: 108408. [PubMed: 32247038]

77. Yu Y, Xu L, Qi L, Wang C, Xu N, Liu S, Li S, Tian H, Liu W, Xu Y, and Li Z. 2017 ABT737 induces mitochondrial pathway apoptosis and mitophagy by regulating DRP1-dependent mitochondrial fission in human ovarian cancer cells. Biomedicine & pharmacotherapy = Biomedecine & pharmacotherapie 96: 22–29. [PubMed: 28963947]

Author Manuscript Author Manuscript Author Manuscript Author Manuscript

Key points

- OGG1 inhibitor SU0268 facilitates antibacterial immunity in PA14 infection.
- SU0268 mitigates bacterial infection via an mtDNA-mediated cGAS pathway.
- SU0268 attenuates lung injury caused by PA14 infection *in vivo*.

Author Manuscript Author Manuscript Author Manuscript Author Manuscript

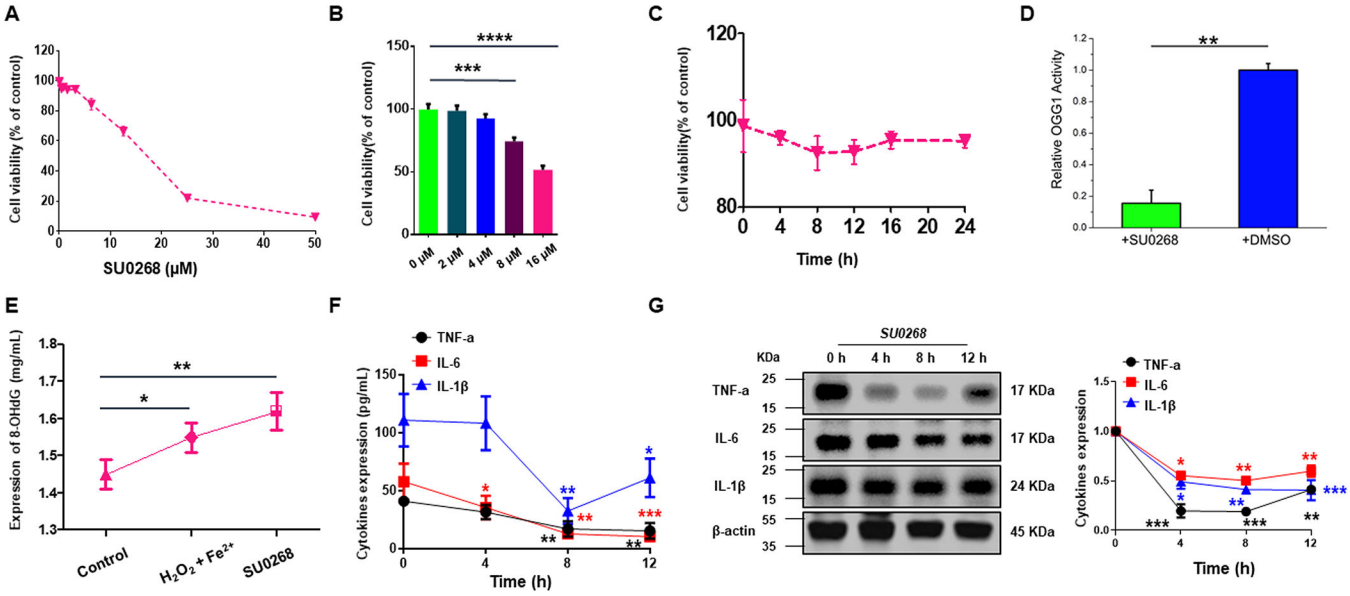

FIGURE 1.

The chemical inhibitor SU0268 suppresses OGG1's activity and inflammatory response in cell culture. **(A)** Cell viability detected by MTT assay. MH-S macrophages were treated with SU0268 (50, 25, 12.5, 6.25, 3.125, 1.5625, 0.78, 0.39 μM) for 24 hours and IC50 was calculated with GraphPad 7.0. (**B**) Cell viability evaluated after treating cells with SU0268 at 0, 2, 4, 8, 16 μM, respectively. (**C**) Cell viability was further evaluated by MTT at 2 μM for indicated times. **(D)** Endogenous OGG1 activity in lysates prepared from MH-S cells (0.1 mg/mL total protein) was measured using a previously described fluorescence assay (23). **(E)** MH-S Cells were cultured in the presence of SU0268 (1 μM) for 36 hours or treated with H_2O_2 (5 mM) and Fe^{2+} (100 μM) for 1 hour. Total DNA was then isolated and digested with nuclease P1 prior to measurement of 8-oxoG using a commercial 8-hydroxy 2-deoxyguanosine ELISA kit. The anti-inflammatory effect of SU0268 was evaluated by quantifying the expression level of TNF-α, IL-1β and IL-6 by using ELISA **(F)** and **(G)** western blotting after treatment with SU0268 (2 μM) for 0, 4, 8, 12 hours.

Author Manuscript Author Manuscript Author Manuscript Author Manuscript

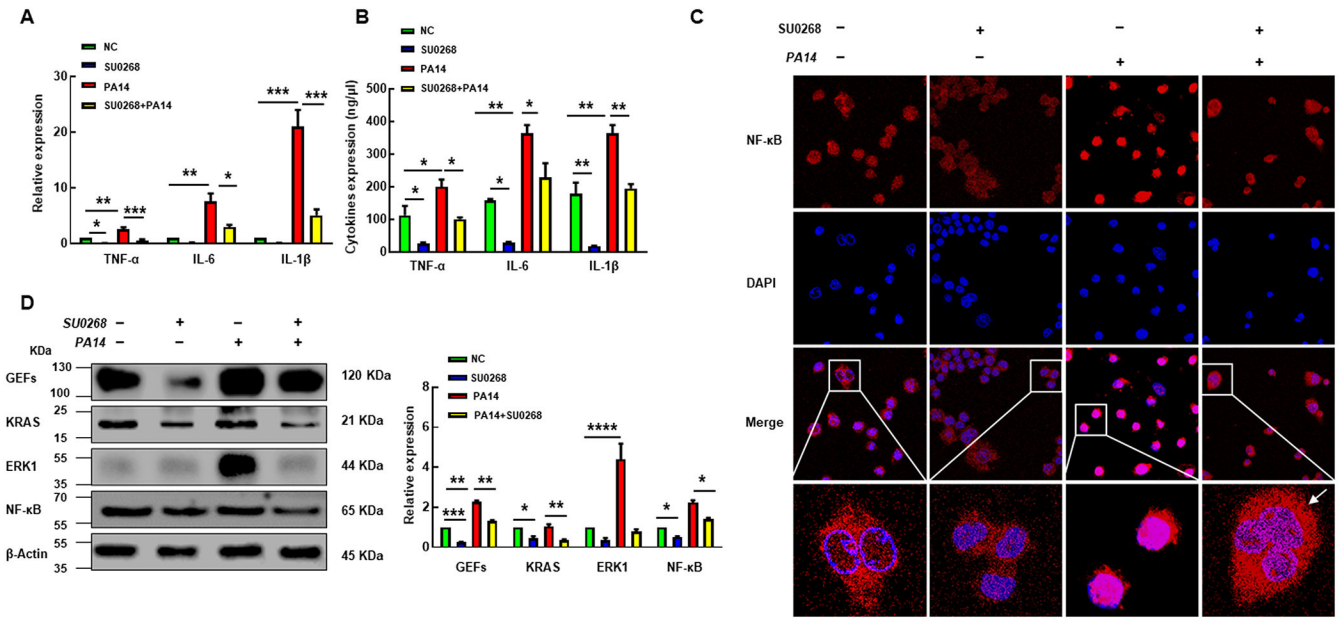

FIGURE 2.

SU0268 inhibits inflammatory responses in MH-S cells via OGG1- GEFs/KRAS-NF-κB axis. MH-S cells were treated with SU0268 (2 μM) for 8 h (the control group received an equal amount of 100% ethanol), then infected with PA14 for 2 h. Anti-inflammatory activity of SU0268 was analyzed by measuring the expression of TNF-α, IL-1β and IL-6 by qPCR **(A)** and ELISA **(B)**. The activation of NF-κB was detected by immunofluorescence **(C)** (arrows indicating cytoplasmic NF-κB staining, the typical cells were enlarged and placed on the bottom). **(D)** The proteins expression levels of OGG1-GEFs/KRAS-NF-κB axis were determined by western blotting.

Author Manuscript Author Manuscript Author Manuscript Author Manuscript

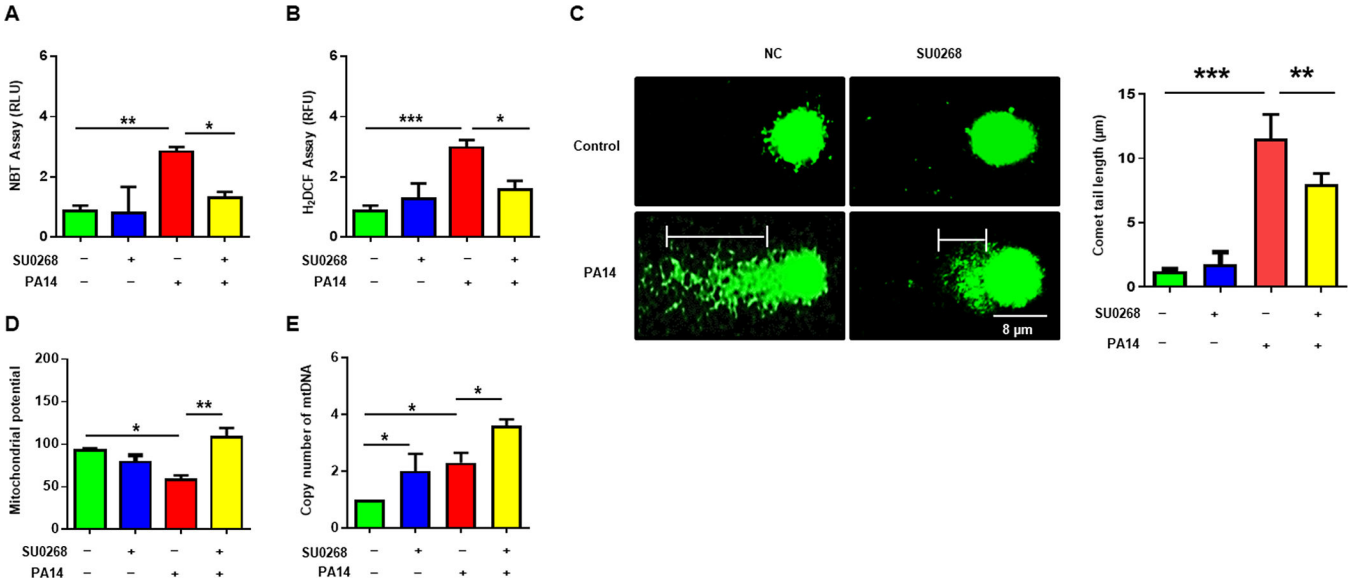

FIGURE 3.

SU0268 promotes mtDNA release into the cytoplasm after ROS-induced DNA damage in response to *P. aeruginosa* infection. MH-S cells were treated with SU0268 (2 μM) for 8 h (the control group received an equal amount of 100% ethanol), then infected with PA14 for 2 h. The ROS products were measured by NBT assay (**A**) and H_2DCF assay **(B)** according to the manufacturer's instructions. (**C**) DNA strand breaks damage were detected by comet assay, and the tail length of damaged DNA was measured with CLSM. (**D**) Mitochondrial membrane potential was assessed by JC-1 fluorescence assay. (**E**) Mitochondrial DNA was extracted and mtDNA copy numbers were analyzed by qPCR.

Author Manuscript
Author Manuscript
Author Manuscript
Author Manuscript

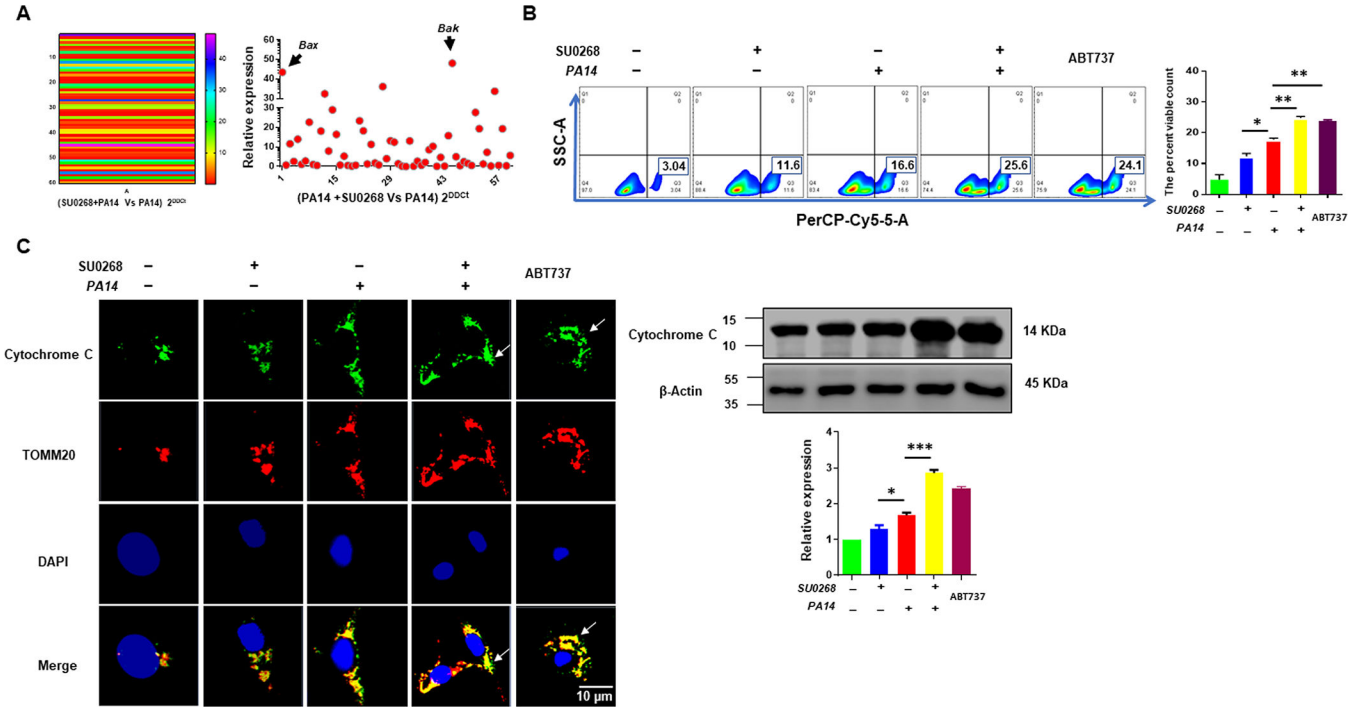

FIGURE 4.

SU0268 promotes mtDNA release dependent on the BAK/BAX axis. MH-S cells were treated with SU0268 (2 μM) for 8 hours (the control group received an equal amount of 100% ethanol), subsequent infection with PA14 for 2 hours. (**A**) 60 genes involved in mtDNA release and mitochondrial function were quantified by using qPCR microarray, heat maps and red dots in scatter plot are used to indicate differential expression of genes (more than two-fold change and $p<0.05$ by Student's t-test, respectively, each color of 1–60 represents the expression of one gene, primers are shown in Supplementary Table S2). (**B**) Cell apoptosis was measured by flow cytometry, ABT737, as a positive control, has been identified to cause apoptosis (77). (**C**) Released cytochrome c was detected by immunofluorescence (arrows indicating typical released cytochrome c) and western blotting (Right panel).

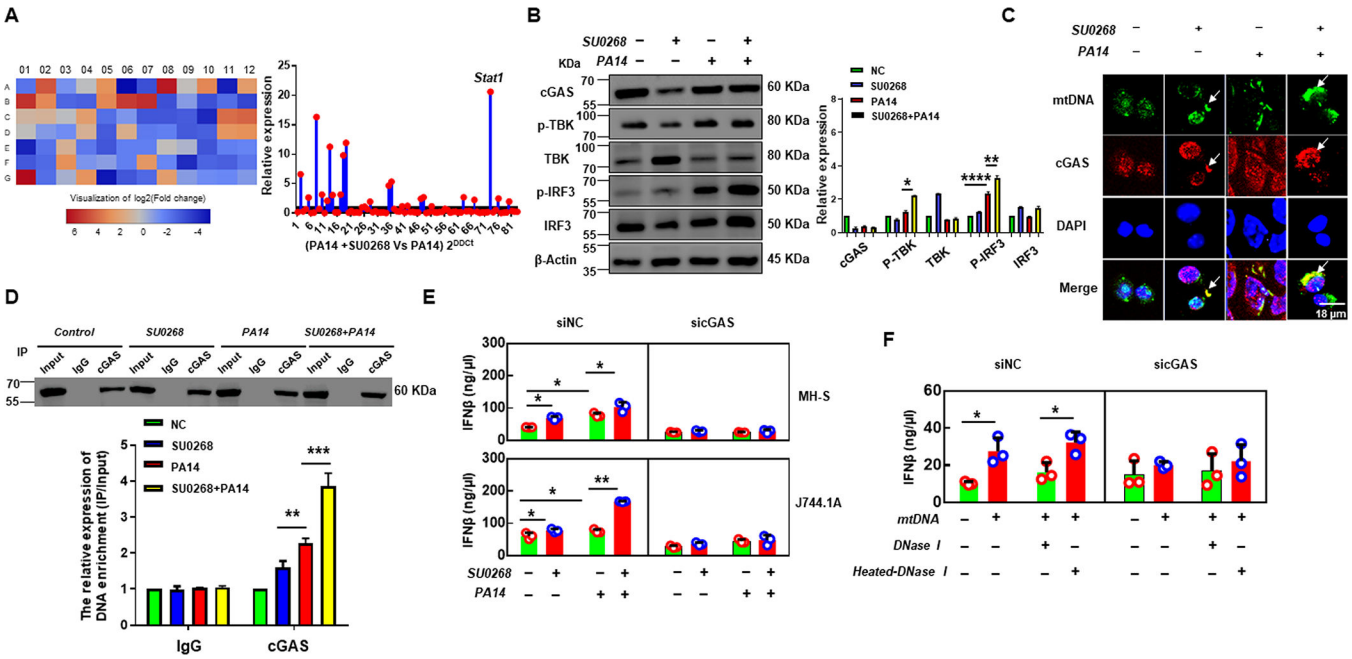

FIGURE 5.

Increased release of mtDNA activates the cGAS pathway by directly binding cGAS protein to manipulate type I IFN responses. MH-S cells were treated with SU0268 (2 μM) for 8 hours (the control group received an equal amount of 100% ethanol), subsequent infection with PA14 for 2 hours. (**A**) RT^2 Profiler PCR inflammation & immunity crosstalk array was used to identify key regulatory genes (330231 PAMM-181Z, QIAGEN, USA). Heat maps and red dots in scatter plots are used to indicate differential expression of genes (more than two-fold change and $p<0.05$ by Student's t-test), respectively, each color of A01-G12 represents the expression of one gene. (**B**) The expression level of proteins (cGAS, p-TBK, TBK, p-IRF3, and IRF-3) were quantified through Western blotting. (**C**) Co-localization of mtDNA and cGAS was detected by immunofluorescence (arrows indicating typical co-localization of mtDNA and cGAS). **(D)** Mitochondria DNA that was bound to cGAS was analyzed by immunoprecipitation, then quantified by qPCR. **(E)** MH-S cells and J744.1A were transfected with cGAS siRNA for 48 h (negative siRNA as control) by using Lip RNAiMAX Reagent, then treated with SU0268 for 8 h (pure ethanol as control), followed by PA14 infection for 2 h. The expression level of IFNβ was determined by ELISA (42400–1, R&D Systems) according to the manufacturer's instructions. **(F)** Mitochondria DNA deletion and replenishment assay were performed in J744.1A cells as previously described (26). J744.1A cells that deleted mtDNA were transfected with cGAS siRNA (Negative siRNA as control) for 36 hours and subsequently treated with PBS or DNAase I or heated-DNAase I for 4 hours, then mtDNA was replenished for 12 hours in pretreated PBS group by using Lip RNAiMAX Reagent, and the expression levels of IFNβ was analyzed by ELISA.

Author Manuscript Author Manuscript Author Manuscript Author Manuscript

Author Manuscript Author Manuscript Author Manuscript Author Manuscript

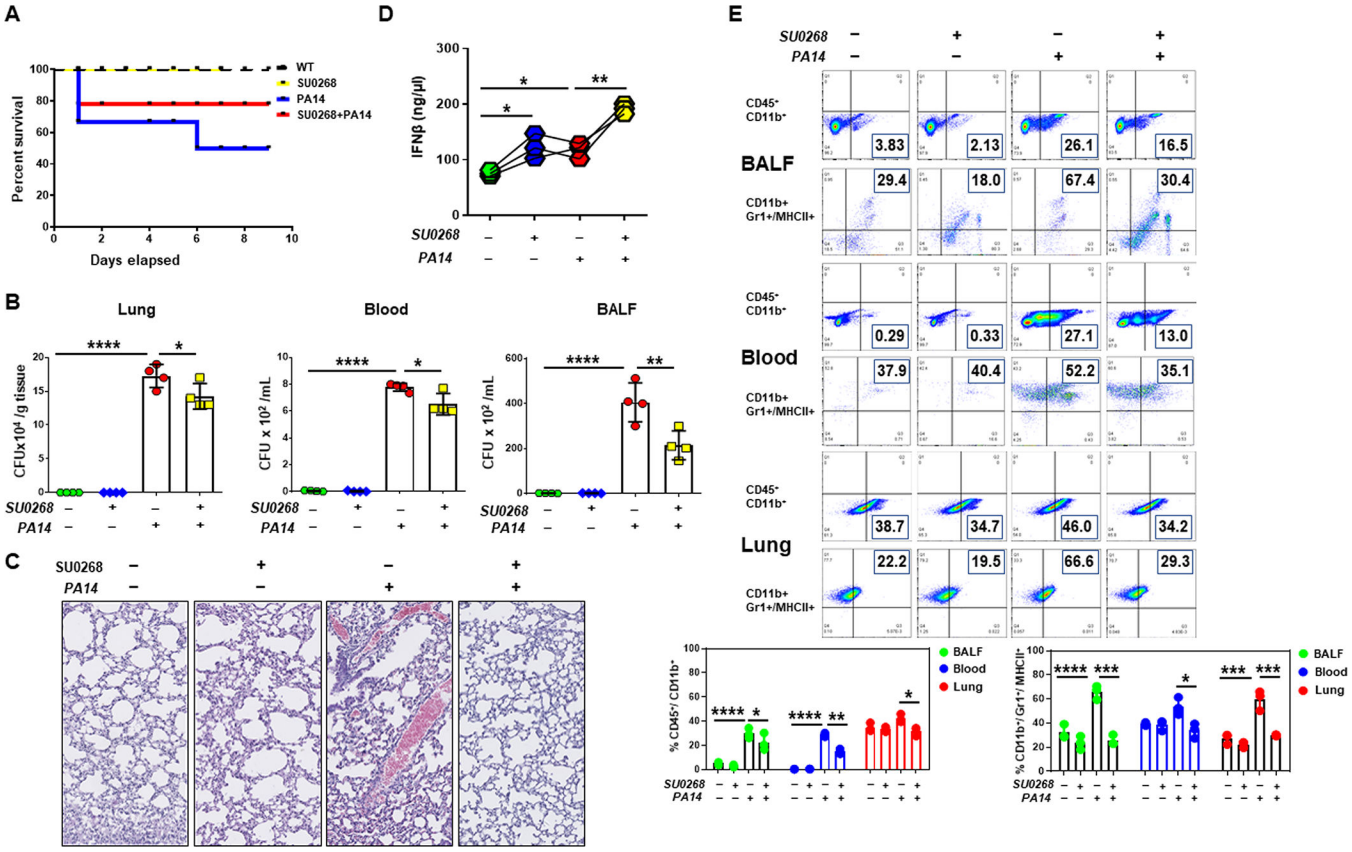

FIGURE 6.

Small-molecule inhibitor of OGG1 significantly down-regulates pro-inflammatory responses and mitigates bacterial infection. Mice treated with SU0268 (10mg/kg) for 12 h and control mice without SU0268 treatment (n = 9) were intranasally challenged with PA14 at 6×10^6 CFU (uninfected WT and SU0268 as a control) and observed up to 9 days. (**A**)The survival test is represented by Kaplan-Meier survival curves, and the results showed that pretreated with SU0268 increased survival rates compared with PA14 infection without SU0268 pretreatment ($p = 0.0925$; 95% confidence interval, n = 9 for each group). (**B**) Colony formation unit assay was used to count the number of bacteria in the lung, blood and BALF at 9 days after infection. **(C)** H&E staining was used to assess lung injury in mice (photograph is magnified 20 times). (**D**) ELISA was performed to determine the expression level of IFNβ in the mouse primary BMDM cells. (**E**) 10,000 cells that were stained by indicated antibodies were collected, the percentages of the myeloid progenitor cells (Stained $CD45^+/CD11b^+$ cells / total cells) and neutrophils (Stained $CD11b^+/Gr1^+/MHCII^+$ cells / total cells) in mouse BALF, blood and lung were detected by flow cytometry.

Author Manuscript Author Manuscript Author Manuscript Author Manuscript

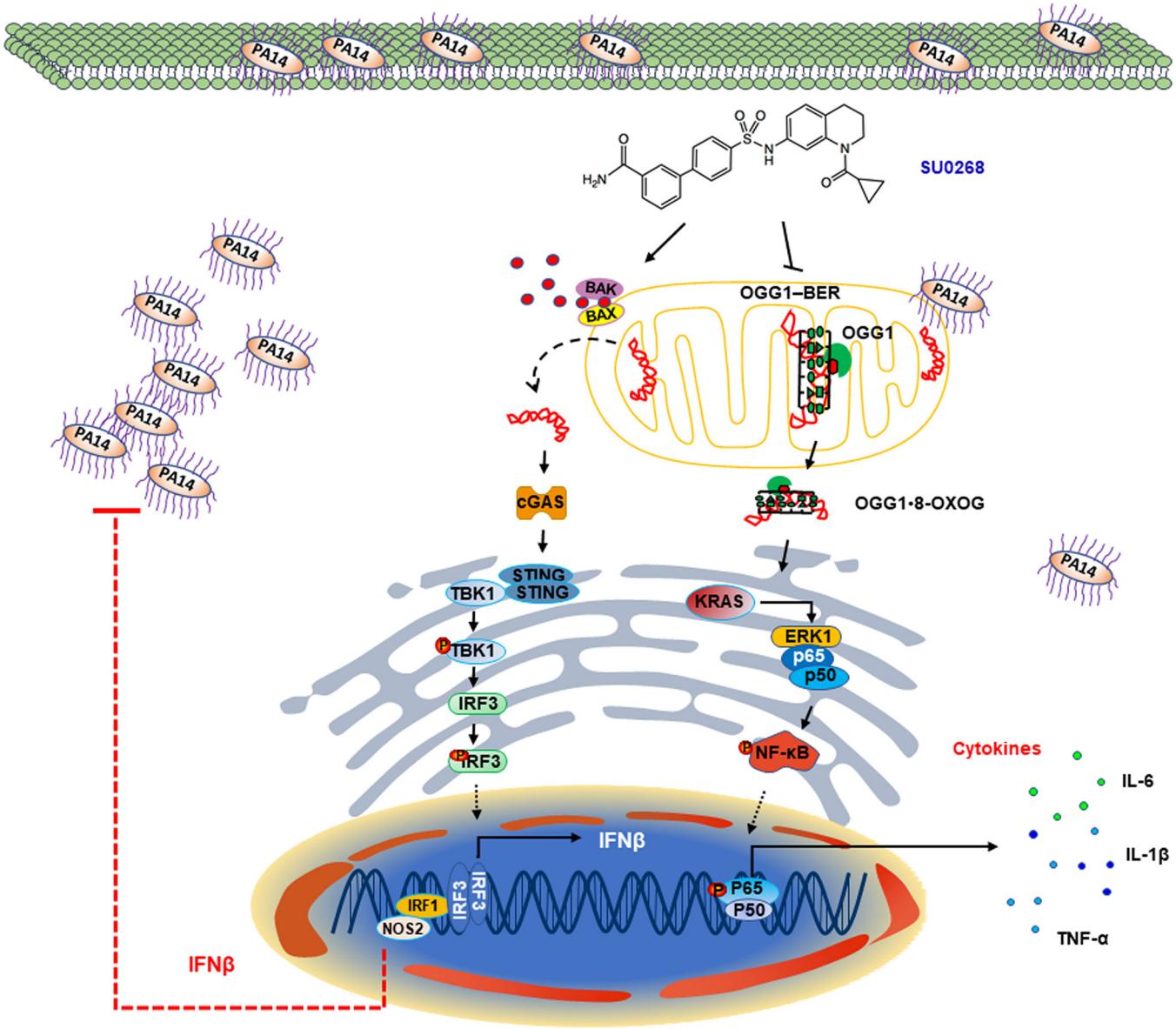

FIGURE 7.

Schematic illustration of the signaling pathways in which small-molecule inhibitor of OGG1 orchestrates inflammatory and mtDNA-mediated Type I IFN responses. Normally, PA14 infection triggers increased ROS production and DNA damage, which moderately activates OGG1's damage repair function and induces an excessive inflammatory response by regulation of the KRAS-ERK1-NF-κB axis. Inhibiting the enzymatic activity of OGG1 decreases DNA inflammatory responses. Furthermore, a small-molecule inhibitor of OGG1 elicits massive mitochondrial DNA release into the cytoplasm, which then initiates IFNβ responses by the cGAS-TBK-IRF3-IFNβ circuit. Ultimately, elevated IFNβ mitigates *P. aeruginosa* infection and spread.